IVYSPRING INTERNATIONAL PUBLISHER

International Journal of Biological Sciences

2027; 23(1): 427-443. doi: 10.7150/ijbs.139696

Research Paper

The Foxo4/Tcf12/TGF-β signaling pathway promotes senescence and fibrosis after cisplatin nephrotoxicity

Fang Xu[1], Honglin Li[1], Yu Xiang[1], Yuqing Zeng[1], Yun Han[1], Wenwen Wu[1], Ying Fu[1], Juan Cai[1], Fanghua Li[2], Dongshan Zhang[3], Yu Liu[1]✉, Zheng Dong[1,4]✉

1. Department of Nephrology, Hunan Key Laboratory of Kidney Disease and Blood Purification, The Second Xiangya Hospital of Central South University, Changsha, Hunan, China.
2. Department of Nephrology, The First Affiliated Hospital of Zhengzhou University, Zhengzhou, Henan, China.
3. Department of Critical Care Medicine, The Second Xiangya Hospital of Central South University, Changsha, Hunan, China.
4. Department of Cellular Biology and Anatomy, Medical College of Georgia at Augusta University and Charlie Norwood VA Medical Center, Augusta, GA, USA.

✉ Corresponding authors: Zheng Dong, PhD, Email: zdong@augusta.edu. Yu Liu, PhD, Email: rory@csu.edu.cn.

© 2027 The Author(s). This is an open access article distributed under the Creative Commons Attribution 4.0 International Licence, subject to the Publisher's Terms of Use at https://ivyspring.com/terms.

Received: 2026.06.22; Accepted: 2026.10.10; Published: 2027.01.01

Abstract

Cisplatin, a widely used chemotherapy drug, is notorious for its side-effects in normal tissues, especially nephrotoxicity in the kidney, but the underlying mechanism remains unclear. Foxo4 is an important transcription factor, yet very limited is known about Foxo4 in renal pathophysiology. In this study, using repeated low-dose cisplatin (RLDC) treatment models, we have delineated the role of Foxo4 in the development of chronic kidney problems following cisplatin exposure. Foxo4 was upregulated in both cell and mouse models of RLDC treatment. Renal cell senescence and fibrosis after RLDC treatment were ameliorated in kidney tubule-specific Foxo4-knockout mice, supporting the role of Foxo4 in renal cell senescence and fibrosis. Mechanistically, ChIP-seq analysis suggested the regulation of Tcf12 by Foxo4, and we further verified Foxo4 binding to a specific site (-1568 to -1558 bp) at the gene promoter region of Tcf12 to induce its expression during RLDC treatment. We showed that Tcf12 may enhance senescence and fibrosis by activating TGF-β/Smad3 signaling in renal tubular cells. Finally, these findings were confirmed in renal biopsies of CKD patients. Collectively, these results unveil the Foxo4/Tcf12/TGF-β signaling pathway that promotes renal senescence and fibrosis after cisplatin nephrotoxicity, suggesting new therapeutic targets.

Keywords: Foxo4; Tcf12; TGF-β; cellular senescence; renal fibrosis; cisplatin

Introduction

Cisplatin is a widely used chemotherapy drug, but it has a serious side effect in normal tissues, especially nephrotoxicity in the kidney [1-5]. About one-third of cancer patients receiving cisplatin chemotherapy experience acute kidney injury within days, and a significant portion of the patients develop chronic kidney disease (CKD) years later [4]. The pathogenesis of CKD development after cisplatin exposure remains largely unclear and effective therapeutics are lacking. Nonetheless, it is known post-cisplatin CKD involves maladaptive kidney repair that is characterized by tubular degeneration, chronic inflammation, and fibrogenesis, associated with a gradual decline of renal function [3-5].

Recent studies have demonstrated a critical role of cellular senescence in maladaptive kidney repair after acute injury [6-10]. Specifically, following injury a subset of failed repair tubular cells may become senescent to assume a secretory phenotype leading to the expression and secretion of profibrotic and proinflammatory factors, which stimulate interstitial fibroblasts for scarring or fibrosis [8, 11-14]. In this regard, cellular senescence is a driving factor in maladaptive kidney repair. Our recent work indicates that tubular cell senescence plays an important role in the development of renal fibrosis and CKD after cisplatin nephrotoxicity[15].

Forkhead box o4 (Foxo4) is a member of the forkhead family of transcription factors. Encoded by a gene at the X chromosome (AFX), Foxo4 was originally identified to fuse with zinc finger transcription factor genes in mixed lineage leukemia (MLL) [16]. Foxo4 is expressed in various tissues and cell types, and plays a crucial role in the regulation of oxidative stress, metabolism, cell death, and other cell biologic processes [16]. However, its function and regulation in renal pathophysiology remains largely unknown.

The present study was designed to investigate Foxo4 in maladaptive kidney repair after cisplatin nephrotoxicity. To model the patient treatment regimen, we used the experimental models of repeated low-dose cisplatin (RLDC) [4, 17]. Our results show that RLDC treatment induces Foxo4, which promotes renal senescence, interstitial fibrosis and CKD development after RLDC treatment in mice kidney tubular cells. Mechanistically, Foxo4 induces the expression of Tcf12 transcriptionally. Tcf12 enhances renal senescence and fibrosis by enhancing TGF-β /Smad3 signaling in renal tubular cells. These findings unveil the Foxo4 / Tcf12/ TGF-β signaling pathway that contributes to maladaptive kidney repair after cisplatin nephrotoxicity suggesting new therapeutic targets.

Results

Foxo4 is induced along with renal senescence and fibrosis after RLDC treatment in mice and kidney tubular cells

We initially examined Foxo4 expression during kidney repair in the mouse model of repeated low-dose cisplatin (RLDC) treatment [4, 17]. C57BL/6 mice were intraperitoneally injected with 8 mg/kg cisplatin once a week for 4 weeks (*in vivo* RLDC treatment) to collect kidney tissues 4 weeks later for analysis. These mice had decreases in kidney to body weight ratio (KW/BW) and transcutaneous Glomerular Filtration Rate (tGFR), and an increase in serum creatinine (Scr) (Figure S1A-S1C). In histology, RLDC induced renal tubular damage including tubular dilation, loss of brush border, and cast formation (Figure S1D, S1E). Masson staining showed collagen deposition in renal interstitium in treated mice (Figure S1F, S1G). To localize Foxo4 expression in mouse kidneys, co-staining of Foxo4 and lotus tetragonolobus lectin (LTL, a marker of kidney proximal tubules) demonstrated that Foxo4 was mainly expressed in the nucleus of proximal tubule cells and the staining was markedly increased after RLDC treatment. RLDC also led to a sustained brush border loss in proximal tubules (Figure 1A, 1B). RT–qPCR analysis further detected an increase in *Foxo4* mRNA in post-RLDC kidneys (Figure 1C). Moreover, RLDC induced senescent and fibrotic changes in kidney tissues, as indicated by the increased expression of senescence and fibrosis markers including p16(Cdkn2a), p21(Cdkn1a) and fibronectin (FN) (Figure 1D, 1E). Immunofluorescence of Foxo4 and p16 revealed their colocalization in the nucleus of kidney tubule cells, and both Foxo4 and p16 signals were increased after RLDC treatment (Figure 1F). We further examined an *in vitro* model of RLDC, in which BUMPT (a mouse kidney proximal tubule cell line) cells were incubated with 2uM cisplatin for 7 hours each day for 4 days [18]. Immunofluorescence detected Foxo4 mainly in the nucleus of BUMPT cells and the staining was markedly increased by RLDC treatment (Figure 1G, 1H). RT–qPCR and immunoblot analysis further detected Foxo4 induction in RLDC-treated cells (Figure 1I-1K). In these cells, Foxo4 induction was accompanied by the expression of senescence and fibrosis markers (Figure 1J, 1K). Immunofluorescence of Foxo4 and p16 further revealed their colocalization and induction by RLDC in the nucleus of BUMPT cells (Figure 1L). Furthermore, we investigated human CKD renal biopsies with paracancerous (PC) kidney tissues as control. The basic information of the CKD (n = 6) and cancer (n = 6) patients is presented in Table S1 (Supporting Information). Histology and Masson's trichrome staining showed greater tubular damage, and interstitial fibrosis in CKD kidney tissues than in PC tissues (Figure 1M&1N). Immunohistochemical staining showed greater accumulation of fibrotic proteins (α-SMA, FN) in interstitial tissues surrounding the atrophic renal tubules in CKD kidney tissues than in PC tissues (Figure 1M&1N). Immunohistochemical analyses verified the higher levels of renal FOXO4 expression in CKD kidney tissues than in PC tissues (Figure 1M&1N). Collectively, these data indicate that Foxo4 is induced along with renal senescence and fibrosis in the experimental models of chronic cisplatin nephrotoxicity.

Renal cell senescence and fibrosis after RLDC treatment are ameliorated in PT-Foxo4-KO mice

To determine the functional significance of Foxo4 induction in post-RLDC kidneys, we established a kidney proximal tubule-specific Foxo4-knockout (PT-Foxo4-KO) mouse model (Figure S2A, S2B). Both immunohistochemical and immunoblot analyses verified the lower levels of renal Foxo4 expression in PT-Foxo4-KO mice than in wild-type (PT- Foxo4-WT) mice (Figure S2C–S2F). PT-Foxo4-WT and PT-Foxo4-KO mice were subjected to RLDC treatment for analysis 4 weeks later.

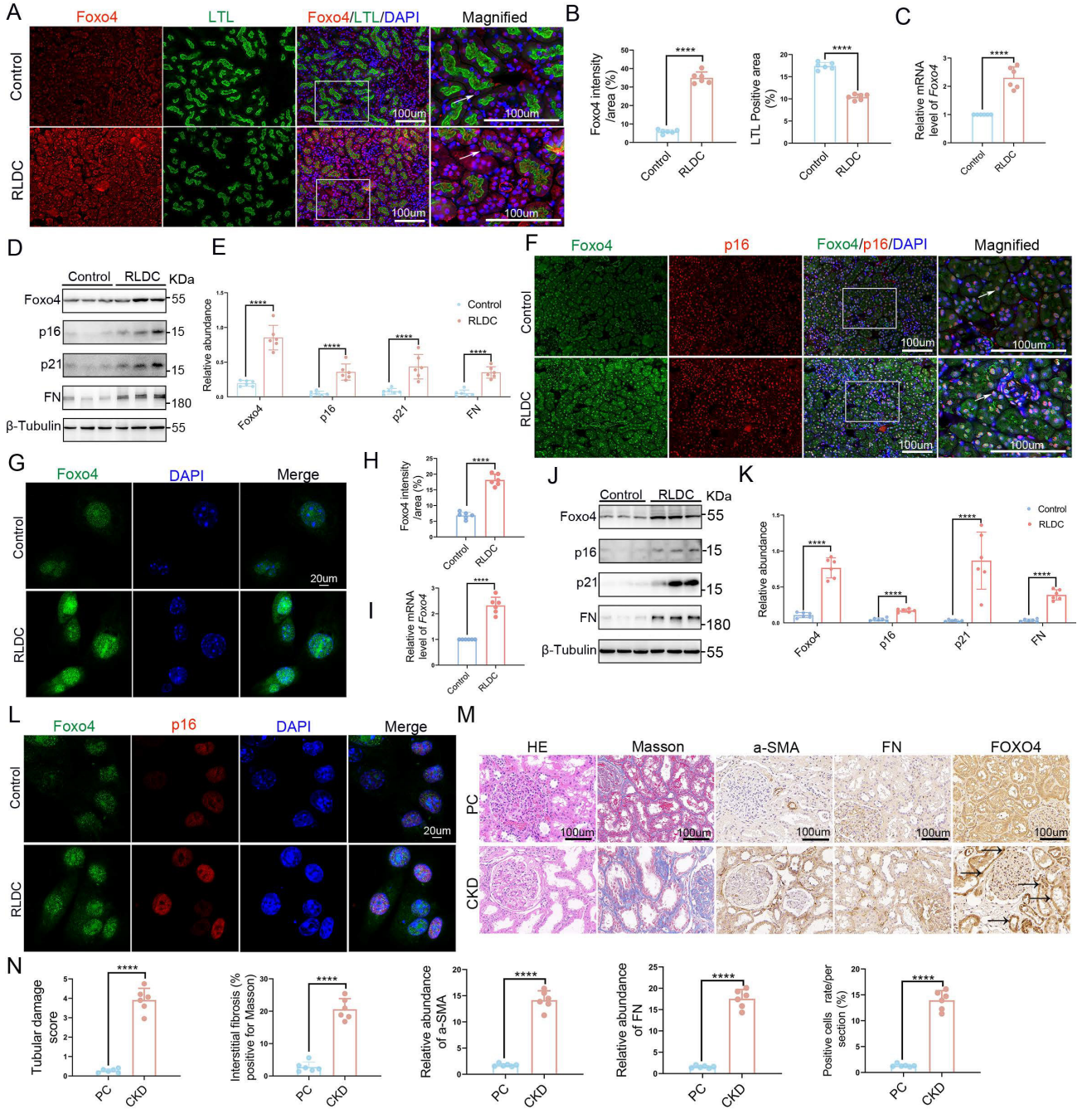


Figure 1. Foxo4 is induced along with renal senescence and fibrosis after RLDC treatment in mice and kidney tubular cells. (A-F) C57BL/6 mice were intraperitoneally injected with 8 mg/kg cisplatin or saline (Control) once a week for 4 weeks (*in vivo* RLDC treatment). At 4 weeks after RLDC, the kidneys were harvested for analysis. (**A**) Foxo4 immunofluorescence (red), LTL staining(green), and DAPI nuclear staining (blue) in kidney tissues. Original magnification x 400. Scale Bar:100μM. (**B**) Quantitative analysis of Foxo4 staining and LTL staining in tubular cells. (**C**) RT-qPCR analysis of *Foxo4* mRNA. (**D**) Immunoblot analysis of Foxo4, p16, p21, and FN protein expression. (**E**) Densitometry of immunoblot bands. (**F**) Foxo4 immunofluorescence (green), p16 staining(red), and DAPI nuclear staining (blue) in kidney tissues. Original magnification x 400. Scale Bar:100μM. **(G-L)** BUMPT cells were incubated with 2uM cisplatin for 7 hours each day for 4 days (*in vitro* RLDC treatment) or left untreated to collected cell lysate for analysis. (**G**) Immunofluorescence of Foxo4 in BUMPT cells. (**H**) Quantitative analysis of Foxo4 staining. (**I**) RT-qPCR analysis of *Foxo4* mRNA. (**J**) Immunoblot analysis of Foxo4, p16, p21 and FN, followed by densitometry of immunoblot bands (**K**). (**L**) Immunofluorescence of Foxo4 (green), p16 staining(red), and DAPI nuclear staining (blue). Scale Bar:20μM. **(M, N)** Human kidney samples from CKD patients and paracancerous (PC) normal kidney tissues. **(M)** H&E staining of renal histology, Masson staining of renal fibrosis, immunostaining of α-SMA, FN and FOXO4. Original magnification x 400. Scale Bar:100μM. **(N)** Quantification of tubular damage, quantification of tubulointerstitial fibrosis, quantification of α-SMA, FN and FOXO4. P values <0.05 were considered significant, with P values presented as follows: NS, P>0.05; *, P<0.05; **, P<0.01; ***, P<0.001; ****, P<0.0001.

RLDC induced decreases in kidney to body weight ratio and tGFR along with increase in Scr, all of which were ameliorated by PT-Foxo4-KO (Figure 2A-2C). PT-Foxo4-KO also alleviated histological damage in RLDC-treated mice (Figure 2D, 2E). Furthermore, renal cell senescence indicated by senescence-associated galactosidase β1 (SA-β-gal) staining and p16 expression, was largely inhibited by PT-Foxo4-KO

(Figure 2D, 2F, 2G). For fibrosis, Masson's trichrome staining was obviously less in PT-Foxo4-KO mice than in wild-type after RLDC treatment (Figure 2H, 2I). Consistently, immunohistochemical staining showed the accumulation of fibrotic proteins (FN, collagen IV, α-SMA) in interstitial tissues surrounding the atrophic renal tubules in post-RLDC mice, which was reduced by PT-Foxo4-KO (Figure 2H, 2J). The staining results were confirmed by immunoblot analysis (Figure 2K, 2L). RLDC treatment induced multiple SASP factors, including *Il-6, Mcp1, Tnf-a*, matrix metalloproteinases 13 (*Mmp*13), and Insulin-like growth factor-binding protein 3(*Igfbp3*), but this induction of *Il-6,* *Mmp*13 and *Igfbp3* was suppressed in PT-Foxo4-KO mice (Figure S2G). Moreover, PT-Foxo4-KO suppressed the induction of pro-fibrotic cytokines, such as platelet-derived growth factor (*Pdgf*) and *Tgf-β1*, in post-RLDC kidneys (Figure S2H). Together, these data show that PT-Foxo4-KO ameliorates renal cell senescence, interstitial fibrosis and CKD development after RLDC treatment, supporting a role of Foxo4 in maladaptive kidney repair.

Foxo4 facilitates renal cell senescence and fibrotic changes in BUMPT cells

To determine the role of Foxo4 *in vitro*, BUMPT cells were transfected with Foxo4 siRNA for knockdown or negative control (NC) siRNA, and then subjected to *in vitro* RLDC treatment. Foxo4 siRNA1 and Foxo4 siRNA3 had significant knockdown effects in immunoblot and immunofluorescence analyses (Figure S3A–S3D). Foxo4 knockdown significantly decreased SA-β-gal staining and the expressions of senescence genes (p16 and p21) during RLDC treatment (Figure 3A-3D). Moreover, it attenuated the expression of fibrotic proteins like FN and Collagen IV (Figure 3C, 3D). Foxo4 knockdown markedly attenuated the expression of multiple SASP factors and pro-fibrotic cytokines during RLDC treatment of BUMPT cells (Figure S3E, S3F). In contrast, overexpression of Foxo4 (Figure S3G–S3I) promoted tubular cell senescence shown by the expression of SA-β-gal, p16, p21, and enhanced the expression of fibrotic proteins (FN and Collagen IV) and following RLDC treatment (Figure 3E-3H). Also, overexpression of Foxo4 significantly elevated the mRNA expression of multiple SASP factors and pro-fibrotic cytokines during RLDC treatment of BUMPT cells (Figure S3J, S3K). These results, consistent with our knockout mouse model study, support a critical role of Foxo4 in renal cell senescence and fibrosis.

Foxo4 interacts with the promoter of Tcf12 to transactivate its expression in RLDC models

Foxo4 is a member of the forkhead family transcription factors. Thus, to delineate the mechanism of Foxo4 function, we analyzed its binding DNA sequences in RLDC-treated cells. BUMPT cells stably transfected with HA-Foxo4-GFP or empty vector were subjected to RLDC treatment or untreated to collect cell samples for ChIP-seq analysis. The analysis identified a total of 8277 DNA sequences with differential Foxo4-binding after RLDC treatment, including 611 at gene promoters with 442 up-regulated and 169 down-regulated (Figure 4A, 4B). In KEGG enrichment analysis, these genes are involved in various pathways, including MAPK and Wnt signaling pathways (Figure 4C). Among the upregulated binding genes, Tcf12 has been reported to promote senescence in chondrocytes[19]. The ChIP-seq image visualized in IGV Genome Browser showed an obviously higher enrichment of Foxo4 at Tcf12 promoter in RLDC cells than in Control cells (Figure 4D). Analysis of the MoLoTool database further suggested a putative Foxo4-binding element (5'-TTTGTTTAGGA -3') in the upstream (-1568 to -1558 bp) promoter region of Tcf12 gene (Figure 4E). We then assessed Foxo4 binding to Tcf12 by chromatin immunoprecipitation (ChIP) assay. As shown in Figure 4F, RLDC treatment induced a 2-fold increase in the binding of Foxo4 to the promoter of Tcf12. We further verified the function of the putative Foxo4-binding element by luciferase promoter reporter assay. As shown in Figure 4G, Foxo4 expression induced the Tcf12 promoter activity, but, when the binding sequence was mutated, it was no more effective. These results indicate that Foxo4 functions as a key transcriptional regulator driving Tcf12 induction.

To further determine the regulation of Tcf12 by Foxo4, we examined the effects of Foxo4 on Tcf12 expression in RLDC models. Tcf12 was induced by RLDC in BUMPT cells (Figure 5A, 5B). Importantly, knockdown of Foxo4 suppressed Tcf12 expression (Figure 5C-5E), whereas overexpression of Foxo4 increased it (Figure 5F, 5G). In mice, both *Tcf12* mRNA and protein were markedly induced after RLDC treatment (Figure 5H, 5I). PT-Foxo4-KO significantly suppressed the expression of Tcf12 in this model (Figure 5J-5L). Together, these results indicate that Foxo4 may induce Tcf12 transcriptionally during RLDC treatment by directly interacting with its -1568 to -1558 bp promoter sequence.

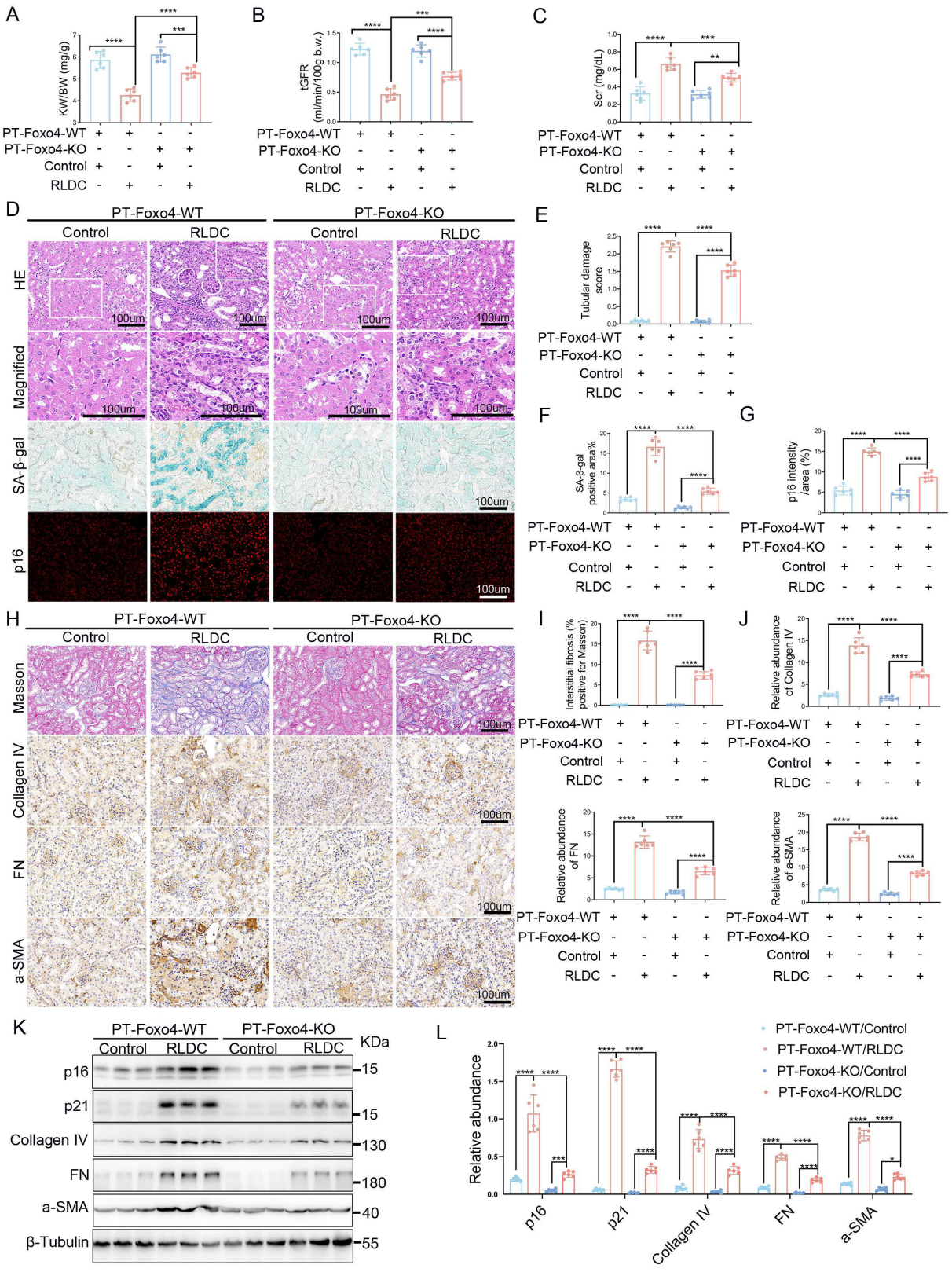


Figure 2. Renal cell senescence and fibrosis after RLDC treatment are ameliorated in PT-Foxo4-KO mice. PT-Foxo4-WT and PT-Foxo4-KO mice were subjected to RLDC or control saline treatment. At 4 weeks after RLDC, body and kidney weights were recorded, glomerular filtration rate (GFR) was measured, and blood and kidney samples were harvested. (**A**) Kidney weight to body weight ratio (KW/BW). (**B**) tGFR. (**C**) Serum creatinine (Scr). (**D**) H&E staining of renal histology, representative images of SA-β-gal staining and Immunofluorescence of p16 (red) in kidney tissues. Original magnification x 400. Scale Bar:100μM. (**E**) Quantification of tubular damage. (**F**) Quantification of SA-β-gal staining. (**G**) Quantitative analysis of p16 staining in tubular cells. (**H**) Masson staining of renal fibrosis, immunostaining of Collagen IV, FN and α-SMA. Original magnification x 400. Scale Bar:100μM. (**I**) Quantification of tubulointerstitial fibrosis in the kidney cortex. (**J**) Quantification of Collagen IV, FN and α-SMA. (**K**) Immunoblot analysis of p16, p21, Collagen IV, FN and α-SMA, followed by densitometry analysis of immunoblot bands (**L**). Data are expressed as mean ± SD (n = 6). P values <0.05 were considered significant, with P values presented as follows: NS, P>0.05; *, P<0.05; **, P<0.01; ***, P<0.001; ****, P<0.0001.

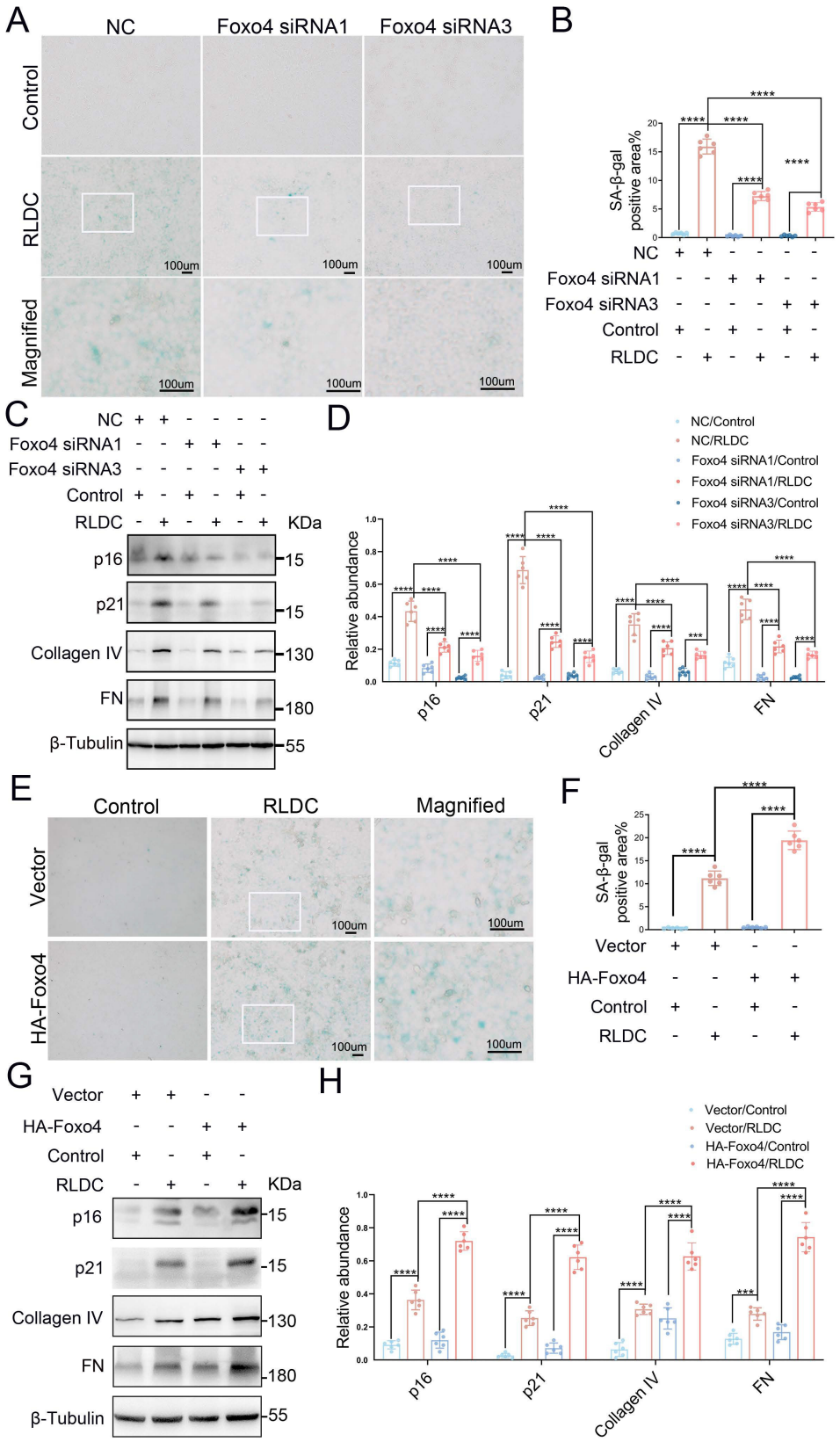


Figure 3. Knockdown of Foxo4 blocks, whereas overexpression of Foxo4 enhances, senescence and fibrotic response during RLDC treatment of kidney tubular cells. (A-D) BUMPT cells were transfected with Foxo4 siRNA or negative control (NC) siRNA, and then subjected to *in vitro* RLDC treatment or left untreated to collect cell lysate for analysis. (**A**) Representative images of SA-β-gal staining. Scale bar:100μm. (**B**) Quantification of SA-β-gal staining. (**C**)Immunoblot analysis of p16, p21, Collagen IV and FN. (**D**) Densitometry analysis of immunoblot bands. **(E-H)** BUMPT cells stably transfected with HA-Foxo4-GFP or empty vector were subjected to *in vitro* RLDC treatment or left untreated to collect cell samples for analysis. (**E**)Representative images of SA-β-gal staining. Scale bar:100μm. (**F**)Quantification of SA-β-gal staining. (**G**)Immunoblot analysis of p16, p21, Collagen IV and FN. (**H**) Densitometry analysis of immunoblot bands. Data are expressed as mean ± SD (n = 6). P values <0.05 were considered significant, with P values presented as follows: NS, P>0.05; *, P<0.05; **, P<0.01; ***, P<0.001; ****, P<0.0001.

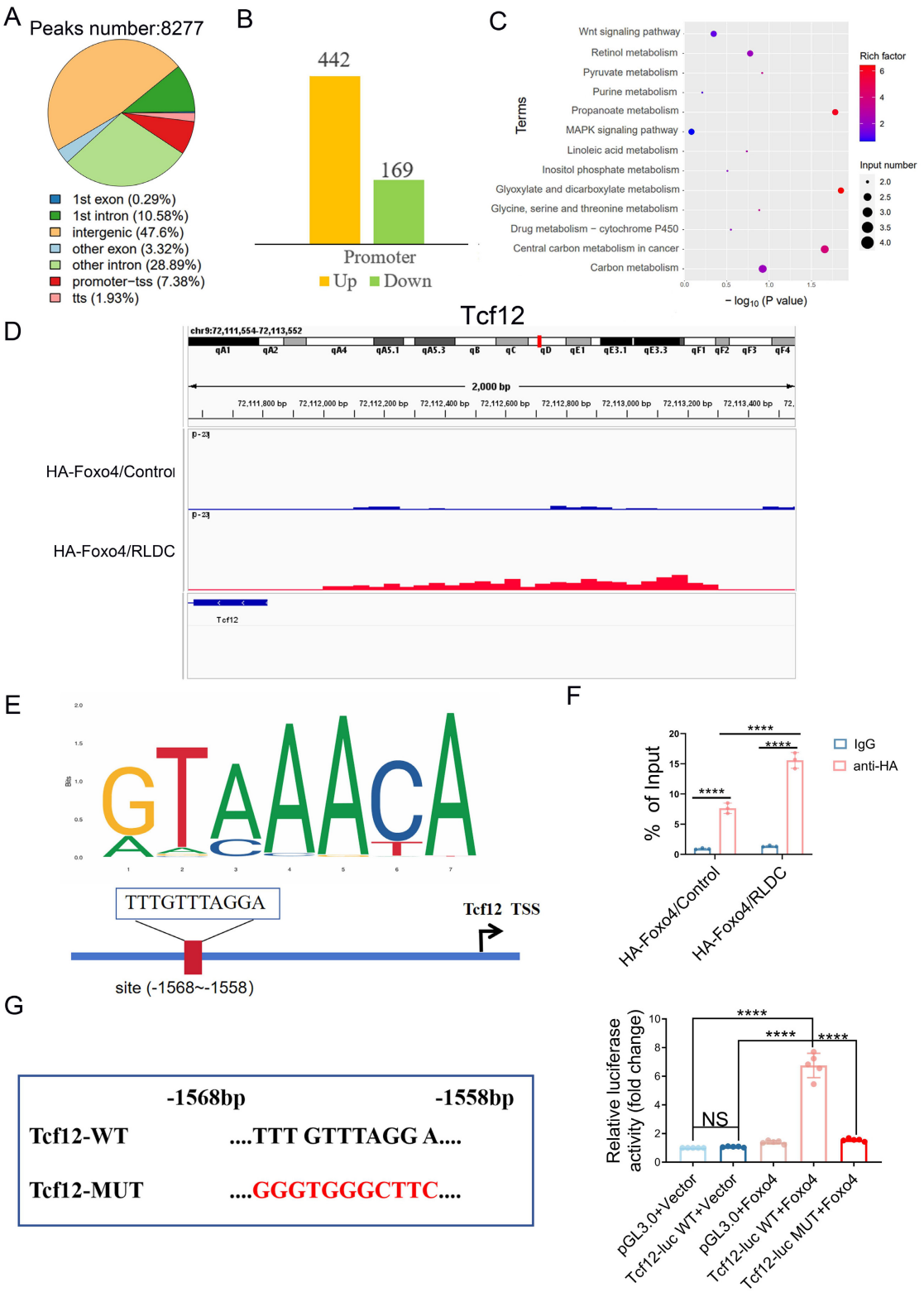


Figure 4. Identification of Tcf12 as a downstream target of Foxo4 during RLDC treatment. BUMPT cells stably transfected with HA-Foxo4-GFP or empty vector were subjected to RLDC treatment or control incubation. Cell lysate was then collected for ChIP-seq analysis to probe Foxo4-binding DNA sequences and RLDC-induced changes. (**A**) ChIP-seq results showing that total 8277 peaks were up- or down-regulated in RLDC versus Control group, and the distribution of these peaks on gene structural elements. (**B**) The number of genes showing RLDC-induced changes in Foxo4 binding to their promoters. (**C**) KEGG enrichment pathways of the genes with differential peaks after RLDC treatment. (**D**) ChIP-seq image of Tcf12 visualized in IGV Genome Browser. (**E**) The putative Foxo4-binding element (5'-TTTGTTTAGGA -3') on the upstream promoter region of Tcf12 gene. (**F**) ChIP assay of Foxo4 binding to Tcf12 promoter sequence after RLDC treatment. Data are expressed as mean ± SD (n = 3). P values <0.05 were considered significant, with P values presented as follows: NS, P>0.05; *, P<0.05; **, P<0.01; ***, P<0.001; ****, P<0.0001. (**G**) Promoter reporter assay to verify the function of the putative Foxo4-binding element. Tcf12 promoter region and its Foxo4-binding site mutated sequence were cloned into pGL3 for transfection into 293t cells to collect lysate 24 hours later for luciferase assay. Data are expressed as mean ± SD (n = 5). P values <0.05 were considered significant, with P values presented as follows: NS, P>0.05; *, P<0.05; **, P<0.01; ***, P<0.001; ****, P<0.0001.

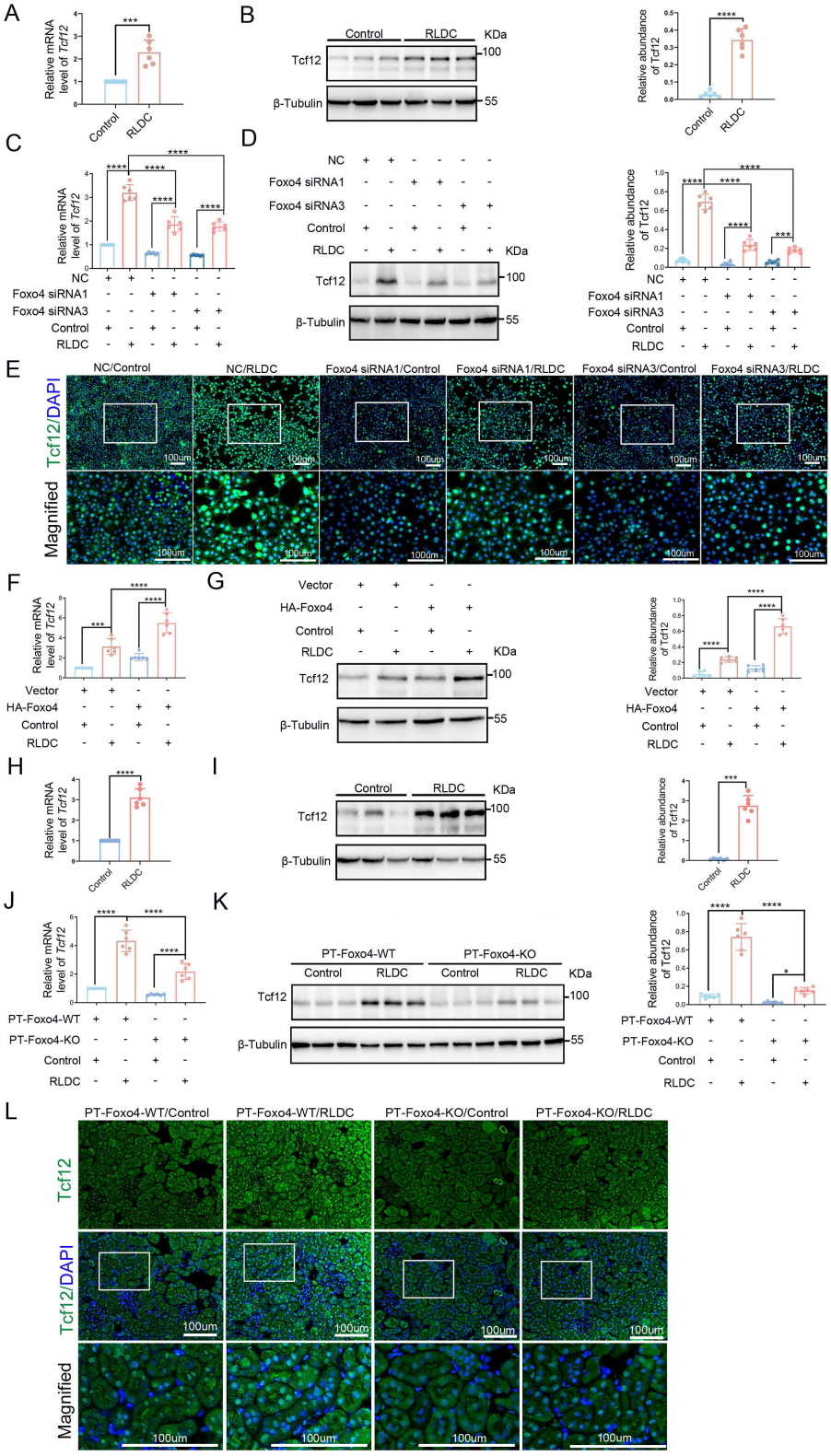


Figure 5. Foxo4 mediates Tcf12 induction following RLDC treatment in kidney tubular cells and in mice. (A, B) BUMPT cells were subjected to *in vitro* RLDC treatment or untreated to collect cell samples for analysis. (**A**) RT-qPCR analysis of *Tcf12* mRNA. (**B**) Immunoblot analysis of Tcf12 with densitometry. **(C-E)** BUMPT cells transfected with Foxo4 siRNA or NC siRNA, and then subjected to RLDC treatment or untreated to collect cell samples for analysis. (**C**) RT-qPCR analysis of *Tcf12* mRNA. (**D**) Immunoblot analysis of Tcf12 with densitometry. (**E**) Immunofluorescence of Tcf12 in BUMPT cells. Scale bar:100μm. **(F, G)** BUMPT cells stably transfected with HA-Foxo4-GFP or empty vector were subjected to RLDC treatment or untreated to collect cell samples for analysis. (**F**) RT-qPCR analysis of *Tcf12* mRNA. (**G**) Immunoblot analysis of Tcf12 with densitometry. **(H, I)** C57BL/6J mice were subjected to *in vivo* RLDC treatment to collect samples for RT-qPCR analysis of *Tcf12* mRNA (**H**) and immunoblot analysis of Tcf12 (**I**). **(J-L)** PT-Foxo4-WT and PT-Foxo4-KO mice were subjected to RLDC treatment to collect blood and kidney samples for analysis. (**J**) RT-qPCR analysis of *Tcf12* mRNA in kidney tissues. (**K**) Immunoblot analysis of Tcf12 with densitometry. (**L**) Immunofluorescence of Tcf12 in mouse kidney tissues. Scale bar:100μm. Data are expressed as mean ± SD (n = 6). P values <0.05 were considered significant, with P values presented as follows: NS, P>0.05; *, P<0.05; **, P<0.01; ***, P<0.001; ****, P<0.0001.

Tcf12 mediates the enhancing effects of Foxo4 on senescence and fibrosis in RLDC-treated BUMPT cells

We then examined the role of Tcf12 in RLDC-induced senescence and fibrotic changes in BUMPT cells. RT-qPCR and immunoblotting verified Tcf12 knockdown with siRNA1 and siRNA2 (Figure S4A-S4C). Importantly, knockdown of Tcf12 decreased the expression of senescence markers, including SA-β-gal, p16 and p21 following RLDC treatment (Figure S4D, S4E). Knockdown of Tcf12 also suppressed the expressions of fibrotic proteins (FN and Collagen IV) (Figure S4F, S4G). Conversely, overexpression of Tcf12 markedly boosted the expressions of the marker proteins of senescence and fibrosis (Figure S5A-S5G). These data support a role of Tcf12 in senescence and fibrosis in RLDC-treated BUMPT cells.

We further determined if the pro-senescence and pro-fibrosis effects of Foxo4 was dependent on Tcf12. To this end, we compared the effects of Foxo4 overexpression in Tcf12 knockdown and control BUMPT cells. Foxo4 overexpression and Tcf12 knockdown in transfected cells were verified by immunoblotting (Figure 6A, 6B). Importantly, Foxo4 overexpression increased the expression of senescence and fibrosis marker proteins, which was suppressed by Tcf12 knockdown (Figure 6C-6F). Collectively, these data indicate that Tcf12 mediates the promoting effect of Foxo4 on senescence and fibrosis in RLDC-treated renal tubular cells.

Tcf12 and Foxo4 promote TGF-β signaling in cell and mouse RLDC models

TGF-β/Smad signaling is a main driving force in renal fibrosis and maladaptive kidney repair [20-22]. In our experiments, knockdown of Tcf12 suppressed the Smad3 phosphorylation/activation (p-Smad3) and TGF-β1 induction in RLDC-treated BUMPT cells (Figure 7A-7C). In contrast, Tcf12 overexpression enhanced Smad3 activation and TGF-β1 induction (Figure 7D-7F). These results manifest that Tcf12 promoted TGF-β signaling during RLDC-treatment of kidney tubular cells.

We further tested if Foxo4 might enhance TGF-β signaling in RLDC-treated cells and mice. Indeed, knockdown of Foxo4 inhibited the activation of Smad3, accompanied by less TGF-β1 expression during RLDC treatment of BUMPT cells (Figure S6 A, S6B& Figure S3F), whereas Foxo4 overexpression had opposite effects (Figure S6 C, S6D& Figure S3K). Moreover, both Smad3 activation and TGF-β1 expression in post-RLDC kidneys were suppressed in PT-Foxo4-KO mice (Figure S6 E, S6F &Figure S2H). These data demonstrate that Foxo4 enhances TGF-β/SMAD signaling during maladaptive repair after cisplatin nephrotoxicity.

SIS3 ameliorates senescence and fibrotic response during RLDC treatment of kidney tubular cells

To verify the involvement of TGF-β/SMAD signaling in post-RLDC changes, we tested the effects of SIS3, a specific pharmacological inhibitor of SMAD3[23-26]. Blockage of Smad3 activation by SIS3 in RLDC-treated BUMPT cells was verified by immunoblotting of p-SMAD3 (Figure S7A, S7B). Notably, SIS3 decreased tubular cell expression of SA-β-gal following RLDC treatment (Figure S7C, S7D). Immunoblot analysis revealed that SIS3 also inhibited the expressions of senescence and fibrosis marker proteins in RLDC-treated cells (Figure S7E, S7F). These results support a role of TGF-β/SMAD signaling in RLDC-induced senescence and fibrotic response in kidney tubular cells.

SIS3 suppresses the effects of Tcf12 overexpression on senescence and fibrotic response in RLDC-treated BUMPT cells

Finally, we tested the hypothesis that Tcf12 enhanced senescence and fibrotic response via TGF-β/SMAD signaling. For this purpose, we examined the effects of Tcf12 overexpression in the absence or presence of SIS3. Tcf12 overexpression facilitated the Smad3 activation, SIS3 clearly inhibited this change (Figure 8A, 8B). Importantly, Tcf12 overexpression promoted the expression of senescence markers (SA-β-gal, p16, p21) and fibrotic proteins (FN, collagen IV), and this effect was significantly less when TGF-β/SMAD signaling was blocked with SIS3 (Figure 8C-8F). Thus, the Tcf12 effect was largely mediated by TGF-β/SMAD signaling.

Discussion

Cisplatin is a potent chemotherapy drug for cancer treatment, but it induces side-effects including acute and chronic kidney problems. The mechanism leading to chronic cisplatin nephrotoxicity is largely unclear. In the present study, using RLDC models of chronic cisplatin nephrotoxicity, we have demonstrated four major findings: (1) Foxo4 is significantly upregulated during RLDC treatment of kidney tubular cells *in vitro* and mice *in vivo*; (2) Foxo4 promotes renal cell senescence and interstitial fibrosis after RLDC treatment; (3) Mechanistically, Foxo4 interacts with the -1568 to -1558 bp promoter sequence of Tcf12 to induce its expression; and (4) Tcf12 enhances renal cell senescence and interstitial fibrosis by activating TGF-β /Smad3 signaling in renal tubular cells. Together, these findings unveil the Foxo4

/Tcf12/TGF-β signaling pathway in the development of chronic kidney problems after cisplatin chemotherapy, suggesting new therapeutic targets.

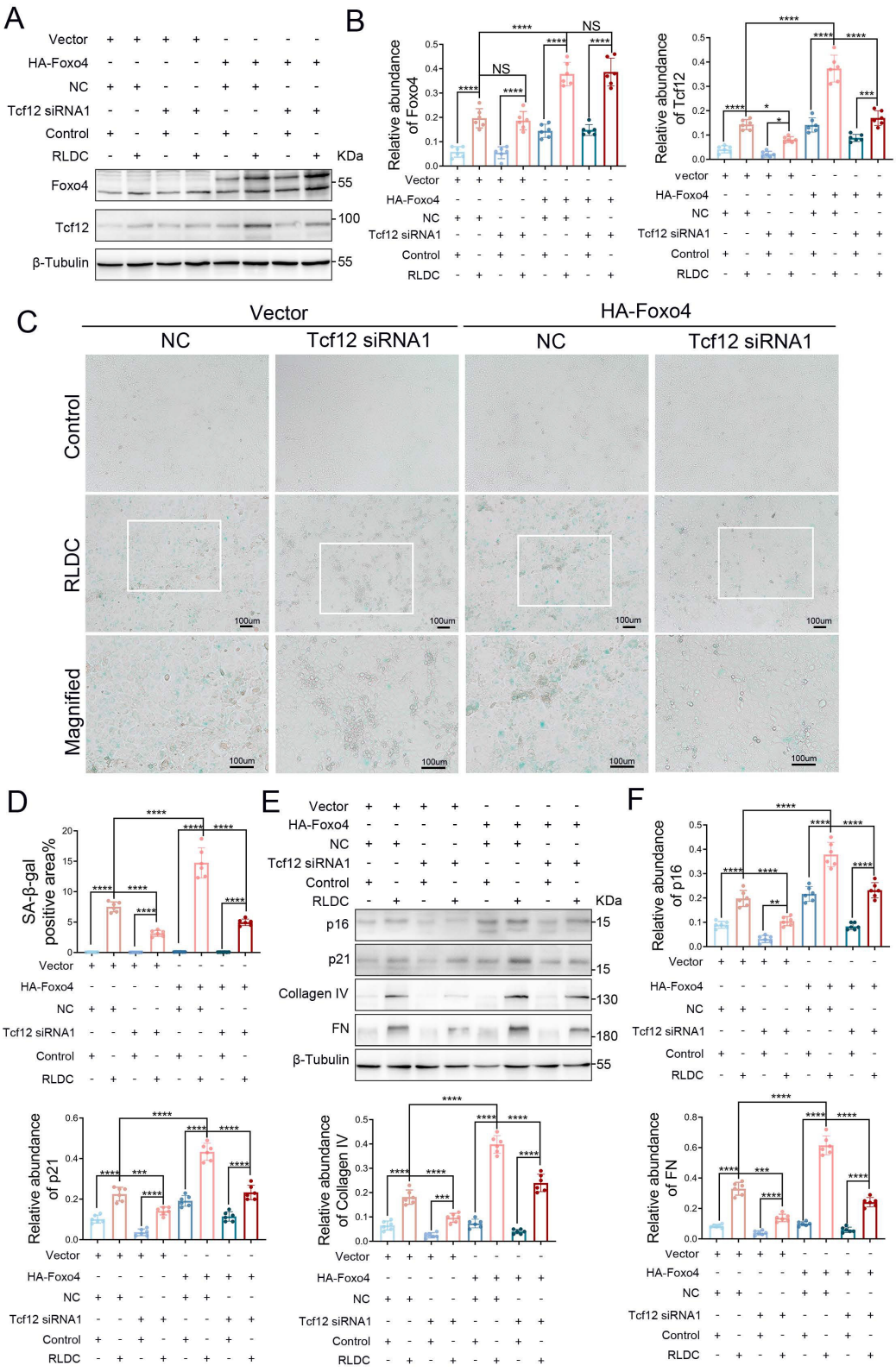


Figure 6. Tcf12 is required for the enhancing effects of Foxo4 on senescence and fibrosis during RLDC treatment. BUMPT cells stably transfected with HA-Foxo4-GFP or empty vector were transfected with Tcf12 siRNA1 or negative control (NC) siRNA, The cells were then subjected to *in vitro* RLDC treatment or left untreated to collect cell lysate for analysis. (**A**) Immunoblot analysis of Foxo4 and Tcf12. (**B**) Densitometry analysis of immunoblot bands. (**C**) Representative images of SA-β-gal staining. Scale bar:100μm. (**D**) Quantification of SA-β-gal staining. (**E**)Immunoblot analysis of p16, p21, Collagen IV and FN. (**F**) Densitometry analysis of immunoblot bands. Data are expressed as mean ± SD (n = 6). P values <0.05 were considered significant, with P values presented as follows: NS, P>0.05; *, P<0.05; **, P<0.01; ***, P<0.001; ****, P<0.0001.

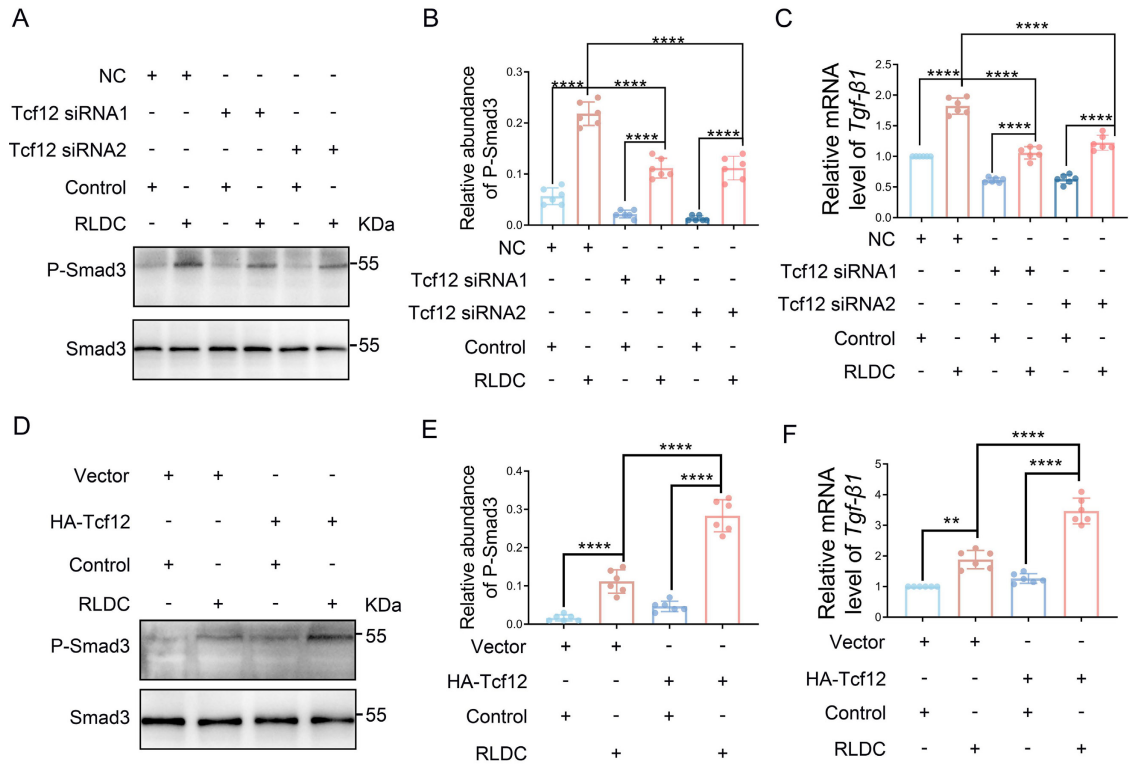


Figure 7. Tcf12 promotes TGF-β signaling during RLDC-treatment of kidney tubular cells. (**A-C**) BUMPT cells were transfected with Tcf12 siRNA or NC siRNA, and then subjected to RLDC treatment or left untreated to collect cell samples for analysis. (**A**) Immunoblot analysis of P-Smad3 with densitometry analysis in (**B**). (**C**) RT-qPCR analysis of *Tgf-β1* mRNA. (**D-F**) BUMPT cells stably transfected with HA-Tcf12-GFP or empty vector were subjected to RLDC treatment or left untreated to collect cell samples for analysis. (**D**) Immunoblot analysis of P-Smad3 with densitometry analysis in (**E**). (**F**) RT-qPCR analysis of *Tgf-β1* mRNA. Data are expressed as mean ± SD (n = 6). P values <0.05 were considered significant, with P values presented as follows: NS, P>0.05; *, P<0.05; **, P<0.01; ***, P<0.001; ****, P<0.0001.

Foxo4 was originally identified in acute myeloid leukemia[16]. However, the majority of recent studies on Foxo4 is in the context of muscle homeostasis[16]. Closely relevant to our present work, several groups demonstrated that Foxo4 may influence aging and age-related diseases[27-30]. In this regard, FOXO4 may directly bind to p53 and thereby activate the p53-dependent transcription of the senescence-associated p21 gene at the site of DNA damage[28], whereas disturbing their specific interaction with competing peptides such as FOXO4-D-Retro-Inverso ameliorates cellular senescence[28]. Our study adds to the understanding of Foxo4's regulation of senescence contributing to the development of renal fibrosis and CKD. Specifically, we observed that Foxo4 induction predominantly in tubular epithelial cells after RLDC treatment in mice. In addition, Foxo4 colocalized with p16-positive tubules, suggesting the intimate correlation between activation of Foxo4 and cellular senescence (Figure 1). Moreover, we found that overexpression of Foxo4 promoted tubular cell senescence shown by the expression of SA-β-gal, p16 and p21, and enhanced the expression of fibrotic proteins, whereas knockdown of Foxo4 attenuated senescence and fibrosis (Figure 3). The role of Foxo4 was further confirmed through the experiments testing renal tubule-specific Foxo4-knockout mice (Figure 2). These observations suggest two temporally and mechanistically distinct aspects of FOXO4 biology: FOXO4 may participate in the cellular response that promotes or stabilizes maladaptive senescence during repeated injury, whereas in cells that have already undergone stable senescence, the FOXO4–p53 interaction becomes an anti-apoptotic, survival mechanism that can be therapeutically disrupted, for example, by FOXO4-DRI.

Foxo4 is known as an important transcription factor[16]. In our study, ChIP-seq analysis suggested that Foxo4 may directly mediate Tcf12 transcription during RLDC treatment of renal tubular cells by binding to the gene promoter of Tcf12. Especially, Knockdown of Foxo4 suppressed Tcf12 mRNA and protein transcription during RLDC treatment. Overexpression of Foxo4 obviously increased it. Notably, knockout of Foxo4 in kidney tubules significantly suppressed the expression of Tcf12 in this model (Figure 5). Our bioinformatics analysis further identified one putative Foxo4 binding site in the gene promoter region of Tcf12. ChIP assay proved that RLDC treatment enhances the binding of Foxo4 to the Tcf12 promoter at positions -1568 to -1558 bp, thereby promoting Tcf12 transcription (Figure 4). To our

knowledge, this is the first report about Foxo4-mediated transcription of Tcf12. Pathologically, Foxo4 mediated transcription of Tcf12 has an important meaning in the development of chronic kidney problems, because this would provide a continuous source of Tcf12 to promote tubular cell senescence and fibrosis.

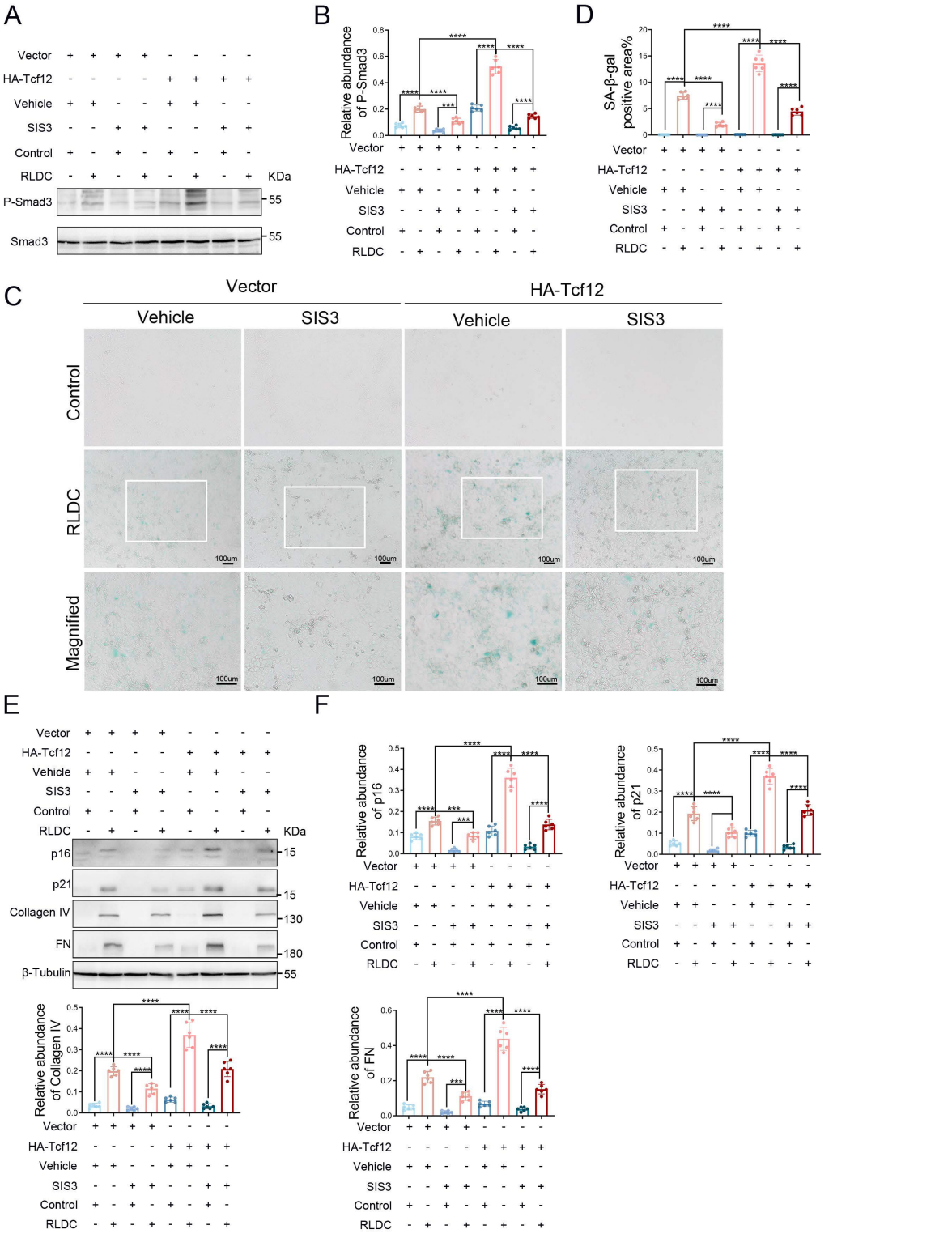


Figure 8. SIS3 suppresses the effects of Tcf12 overexpression on senescence and fibrotic response during RLDC treatment in BUMPT cells. BUMPT cells stably transfected with HA-Tcf12-GFP or empty vector were treated with 5 μM SIS3 or DMSO for 1h, and then subjected to RLDC treatment or left untreated to collect cell lysate for analysis. (**A**) Immunoblot analysis of P-Smad3 with densitometry analysis in (**B**). (**C**) Representative images of SA-β-gal staining. Scale bar:100μm. (**D**) Quantification of SA-β-gal staining. (**E**) Immunoblot analysis of p16, p21, Collagen IV and FN with densitometry analysis in (**F**). Data are expressed as mean ± SD (n = 6). P values <0.05 were considered significant, with P values presented as follows: NS, P>0.05; *, P<0.05; **, P<0.01; ***, P<0.001; ****, P<0.0001.

Our work aligns with previous research identifying Tcf12 as a key molecule in cellular senescence. TCF12 promotes chondrocyte aging by upregulating CXCR4 with consequent TGF-β signaling [19]. In our study, knockdown of Tcf12 alleviated the expression of senescence markers, including SA-β-gal, p16 and p21 following RLDC treatment (Figure S4). Conversely, overexpression of Tcf12 markedly enhanced the expressions of the marker proteins of senescence (Figure S5). These and other results demonstrate that Tcf12 promotes cellular senescence in our model in the kidney. However, the mechanism by which Tcf12 regulates cellular senescence has aroused our immense interest.

Transforming growth factor-β (TGF-β) is a pleiotropic cytokine in the polypeptide superfamily, which plays a central role in the fibrotic process[31-33]. Among its three isoforms (TGF-β1, β2, β3), TGF-β1 is the major pathogenic mediator that initiates and maintains the fibrotic cascade[31-34]. Mechanistically, TGF-β transmits signals through canonical (SMAD-dependent) and non-canonical (SMAD-independent) pathways, ultimately resulting in the sustained activation of fibroblasts, excessive deposition of extracellular matrix (ECM), and progressive destruction of tissue structure[31-34]. Although not secreted by all senescent renal cells, TGF-β1 is generally regarded as a typical component of the senescence-associated secretory phenotype (SASP). In the context of senescence, TGF-β1 may act as a bidirectional activator, which, after being secreted by senescent cells, further induces senescence in surrounding cells. TGF-β1 locally secreted by podocytes can transcriptionally activate p21 and promote p16 nuclear translocation in a Smad3-dependent manner, thereby leading to pro-senescent changes in glomerular endothelial cells [35-37]. Since cellular senescence and TGF-β1 secretion are not always synchronously activated, there must be other regulatory factors involved in this process [36]. Interestingly, our study also found that the TGF-β signaling pathway is involved in the pro-senescence mechanism of Tcf12. In our experiments, knockdown of Tcf12 suppressed TGF-β1 induction and Smad3 activation, whereas overexpression exhibited the opposite results (Figure 7). Moreover, Foxo4 enhanced TGF-β/SMAD signaling during maladaptive repair after cisplatin nephrotoxicity (Figure S6). We also revealed that inhibition of Smad3 with SIS3 suppressed renal cell senescence and interstitial fibrosis (Figures 8 & S7). These data demonstrate that Tcf12 promotes TGF-β signaling in cell and mouse RLDC models. Repeated low-dose cisplatin induces both cell death and senescence in kidney tubules. In our study, Foxo4 induced the expression of Tcf12 transcriptionally, which promoted renal senescence by enhancing TGF-β /Smad3 signaling in renal tubular cells. Further work needs to investigate whether Foxo4 regulates tubular cell death or the balance between cell death and senescence.

In summary, we have provided the first evidence that Foxo4 has a key role in renal cell senescence and interstitial fibrosis. Mechanistically, Foxo4 transactivates Tcf12 expression and, upon induction, Tcf12 enhances senescence and interstitial fibrosis by activating TGF-β /Smad3 signaling. Therefore, inhibition of Foxo4/Tcf12 may protect kidneys from chronic nephrotoxicity during cisplatin chemotherapy.

Materials and Methods

Animals

All mice were maintained in a specific pathogen-free facility at 22–25°C under a light–dark cycle with free access to a standard rodent diet and water. All animal procedures conformed to the NIH Guide for the Care and Use of Laboratory Animals and were approved by the Institutional Animal Care and Use Committee of the Second Xiangya Hospital, Central South University (Approval No. 2022418).

The mouse model of proximal tubule Foxo4 KO was established by Cre-Lox recombination as before[38, 39]. Briefly, female mice with floxed Foxo4 alleles (Foxo4-$X^{flox}X^{-}$ GGT-cre- mice from The Cyagen Biosciences Inc , SuZhou, JiangSu, China) were crossed with male Gamma-glutamyltransferase -Cre transgenic mice (Foxo4-X-Y GGT-cre+ mice from Shanghai Model Organisms, Shanghai, China) to produce littermate proximal tubule Foxo4 wild-type (PT- Foxo4-WT) and PT- Foxo4-KO (Foxo4-X^{flox}Y GGT-cre+) mice or produce heterozygous female offspring (Foxo4-$X^{flox}X^{-}$ GGT-cre+) which was further crossed with GGT-cre-X-Y males to produce littermate proximal tubule Foxo4 wild-type (PT- Foxo4-WT) and PT- Foxo4-KO (Foxo4-X^{flox}Y GGT-cre+) male mice (Figure S2A). Each mouse was subjected to three sets of PCR test. The genotype of PT- Foxo4-KO mice was characterized by (1) amplification of the 202-bp DNA fragment for the floxed allele, (2) deficiency of amplification of the 134-bp DNA fragment for the WT allele, and (3) amplification of the 428-bp DNA fragment of the Cre gene (Figure S2B).

Mouse models of RLDC treatment

Mice (male, 8-10 weeks of age) were sorted according to their body weight and randomly assigned to control group and treatment group. The treatment group was injected with 8 mg/kg cisplatin intraperitoneally once a week for 4 weeks, and the

control group was injected with the vehicle solution of saline. At 4 weeks after RLDC treatment, GFR of the mice was measured by transcutaneously monitoring the clearance of FITC-labeled sinistrin as previously [15, 40, 41]. Kidneys and blood samples were then harvested for analysis.

Cell culture and treatment

The Boston University mouse proximal tubular cell line (BUMPT) was originally provided by Drs. Wilfred Lieberthal and John Schwartz at Boston University School of Medicine (Boston, MA). The HA-Foxo4-GFP stably expressed cell line or the HA-Tcf12-GFP stably expressed cell line was generated according to the manufacturer's instructions. Briefly, BUMPT cells were seeded in 24-well plates with DMEM containing 10% FBS and 1% penicillin–streptomycin at 37 °C in 5% CO2. When the cell density reached 30%, HA- Foxo4-GFP virus solution(2uL) or HA- Tcf12-GFP virus solution(4uL), polybrene (2.5ug/mL) were added for infection for 24 h. After that, 3 μg/mL puromycin was added for selection. Lastly, monoclonal cells were selected for stably expressing HA-Foxo4-GFP or HA-Tcf12-GFP.

For RLDC treatment, the cells were incubated with 2uM cisplatin for 7 hours each day for 4 days (*in vitro* RLDC treatment) or left untreated to collected cell lysate for analysis [15, 40, 41].

Human samples

The study was approved by the Review Board of the Second Xiangya Hospital, People's Republic of China (No. KYZ20260019). 12 patients were recruited for this study. All participants were recruited with written informed consent prior to inclusion in the study. Human kidney samples were collected from 6 patients with CKD, or 6 patients with kidney cancers (PC, n = 6) at the Second Xiangya Hospital, Central South University (Table S1, Supporting Information).

Antibodies and reagents

Anti-Foxo4(ab126757), anti-FN (ab2413), anti-α-SMA (ab5694), anti-Collagen IV for immunohistochemistry (ab6586), anti-Tcf12 for immunofluorescence (ab70746) were obtained from Abcam (Cambridge Science Park, Cambridge, UK). Anti- HA-Tag(C29F4), anti-p16 for immunoblotting (29271S), anti-p21(37543S), anti- phosphorylated Smad3 (phosphorylated SMAD family member 3) (9520), anti- Smad3(9523) were purchased from Cell Signaling Technology (Danvers, MA, USA). Anti-β-tubulin(10094-1-AP), anti-Tcf12 for immunoblotting (14419-1-AP) were obtained from Proteintech (Rosemont, IL, USA). Anti-Collagen IV for immunoblotting (YT5768) was purchased from the Immunoway (Suzhou, Jiangsu, China). Anti-p16 for immunofluorescence (C0308) was obtained from Santa Cruz Biotechnology (California, USA). All secondary antibodies for immunoblotting were obtained from Proteintech (Rosemont, IL, USA) and all secondary antibodies for immunofluorescence were obtained from Abcam (Cambridge Science Park, Cambridge, UK). The Foxo4 siRNAs and NC siRNA were synthesized by Ruibo Biology Company (Guangzhou, Guangdong, China). The Tcf12 siRNAs, NC siRNA, HA- Foxo4-GFP virus solutions, and HA- Tcf12-GFP virus solutions were obtained from Heyuan Biology Company (Shanghai, China). SMAD3 phosphorylation inhibitor SIS3 (HY-13013) was purchased from MedChemExpress (Monmouth Junction, NJ).

ChIP sequencing and data analysis

In this study, chromatin immunoprecipitation coupled with next-generation sequencing (ChIP-Seq) was performed in combination with a reference exogenous genome, and library preparation was completed following the method described previously[42, 43]. BUMPT cells stably transfected with HA-Foxo4-GFP or empty vector were subjected to *in vitro* RLDC treatment or untreated to collect cell samples for ChIP-seq analysis. Then cells were harvested and cross-linked with 1% formaldehyde for 10 min at room temperature, and the cross-linking reaction was quenched with 0.125 M glycine. 1×10^7 cell nuclei were resuspended in 1 mL sonication buffer (1 mM EDTA, 10 mM Tris-HCl, pH 7.5). Nuclei were sonicated using a Covaris E220 Focused-ultrasonicator for 30 min. Immunoprecipitation was performed by incubating with antibodies including anti-HA antibody and anti-IgG antibody overnight at 4°C. After subjecting the immunoprecipitated complexes to a series of washes, elution, and de-crosslinking, DNA was extracted using the phenol-chloroform method and quantified with a Qubit 3 fluorometer (Thermo Fisher Scientific). For high-throughput DNA sequencing, libraries were constructed using the VAHTS Universal DNA Library Prep Kit for Illumina V3 (Vazyme Biotech, Nanjing, China, ND607). Library products corresponding to fragments of 200–500 bp were enriched and quantified. Finally, sequencing was performed on the [DNBSEQ-T7RS High-throughput Sequencing Kit (FCL PE150) V3.0, Catalog NO:940-000266-00, MGI Tech Co., Ltd., China] sequencing platform. Reads distribution analysis was performed using RSeQC (version 2.6). Peak calling was conducted using MACS2 (version 2.2.7.1) or epic2 (version 0.0.52). Peak annotation was carried out with Bedtools (version 2.30.0), and peak distribution analysis was performed using deepTools (version 3.5.1).

Differentially binding peaks were identified using csaw (version 1.30.1). Motif analysis was performed using Homer (version 4.9.1). For the annotated genes, both Gene Ontology (GO) analysis and Kyoto Encyclopedia of Genes and Genomes (KEGG) enrichment analysis were implemented using KOBAS software (version 2.1.1), with a corrected P-value < 0.05 set as the cutoff for statistically significant enrichment.

ChIP analysis

BUMPT cells stably transfected with HA-Foxo4-GFP or empty vector were subjected to *in vitro* RLDC treatment or untreated to collect cell samples. ChIP assays were carried out using a ChIP kit (Millipore, Boston, MA, USA). Anti-HA-tag antibody was used to precipitate protein-bound DNA. Mouse IgG was used as a control. Precipitated DNAs were detected by q-PCR using specific primers:

Tcf12 (S1): 5′-ATCCGCTAGTCTTAGTTGG AAACG-3′ (forward), and 5′-AGCCAGTCCCACTTAGGTACATAC-3′ (reverse).

Luciferase assay

The promoter region of Tcf12 (-2000 to 200 relative to the transcription start site) and its putative Foxo4-binding site mutant were separately cloned into pGL3 vector. The plasmids were transfected into 293t cells for 24 h to collect cell lysate [44]. Luciferase activity was measured with the Dual Luciferase Reporter Gene Assay Kit (Beyotime, RG027) according to the manufacturer's instructions.

SA-β-gal staining

SA-β-gal staining was done using the Senescence Detection kit (Abcam, ab65351). In brief, cells or frozen kidney tissue were washed with PBS three times for 5 min each, then incubated with 0.5mL fixative solution for 10-15min at room temperature. The samples were then exposed to the Staining Solution Mix (Staining Solution, Staining Supplement, 20mg/ml X-gal in DMF) at 37 °C without CO_2 for overnight. The samples were then washed three times with PBS. The cells were monitored under a microscope for development of blue color[15].

Reverse transcription quantitative PCR (RT-qPCR)

Total RNA was extracted from BUMPT cells or kidney tissue using the Trizol reagent (TaKaRa, AO70709A), and then reverse-transcribed into first-strand cDNA using the Prime Script FAST RT Reagent kit with gDNA Eraser (TaKaRa, AOF0611A). Next, the cDNA was used as a template with TB green (TaKaRa, AO61621A) and a Light cycler 96 (Roche) with the primer pairs. The sequences of the primer pairs used in real-time PCR are listed in (Table S2, Supporting Information). ΔΔCT values were used to perform the relative quantification. The absolute quantification was carried out according to a standard curve.

Immunoblot analysis

Equal amounts of proteins were loaded on each lane and separated by SDS-PAGE, and then transferred onto a nitrocellulose membrane (Amersham, Buckinghamshire, UK) according to previously described[45]. The blot was then washed in TBST buffer, blocked for 60 minutes in the blocking buffer (5% milk). The blot was then incubated with primary antibodies against Foxo4 (1:1000 dilution), Collagen IV (1:1000 dilution), FN (1:1000 dilution), a-SMA (1:1000 dilution), HA (1:1000 dilution), Tcf12 (1:1000 dilution), phosphorylated Smad3 (1:1000 dilution), Smad3 (1:1000 dilution), p21 (1:1000 dilution), p16 (1:1000 dilution), or β-Tubulin (1:2000 dilution) overnight incubation at 4°C, followed by incubation with secondary antibody (1:5000 dilution) and detection reagents.

Histological analysis and immunostaining

H&E staining was used to analyze renal histology. The tubular damage score of kidneys was performed as previously described[15, 40, 41]. Fibrosis was evaluated by the Masson's trichrome staining. Immunohistochemical analysis was carried out using anti-collagen IV (1:100 dilution), anti-FN (1:50 dilution), anti-Foxo4 (1:100), anti-a-SMA (1:100 dilution) according to the previous protocol [45]. Stained samples were analyzed using an Olympus microscope equipped with UV epi-illumination. For immunofluorescence staining, the sections were incubated with specific primary antibodies (anti-Foxo4 1:100, anti-p16 1:50) overnight at 4°C followed by a secondary fluorescent antibody for 1 hour at 37°C in the dark. DAPI was then added for 3-5 minutes to label cell nuclei and the sections were examined by fluorescence microscopy.

Statistics

All data were presented as means ± SD. Two groups were compared using two-tailed t-tests. One-way ANOVA was used for multiple group comparisons. Kruskal-Wallis test was used for the non-parametric tests for multiple group's comparison. For all statistical tests, P values <0.05 were considered significant, with P values presented as follows throughout the article: NS, P>0.05; *, P<0.05; **, P<0.01; ***, P<0.001; ****, P<0.0001.

Abbreviations

CKD: chronic kidney disease; Foxo4: Forkhead box o4; RLDC: repeated low-dose cisplatin; TIF: tubulo-interstitial fibrosis; Scr: serum creatinine; BW: body weight; KW/BW: Kidney to body weight ratio; tGFR: transcutaneous Glomerular Filtration Rate; LTL: lotus tetragonolobus lectin; Fn: Fibronectin; α-SMA: alpha smooth muscle Actin; PC: paracancerous; p16: p16(Cdkn2a); p21: p21(Cdkn1a); SA-β-gal: senescence-associated galactosidase, β 1; PT-Foxo4-KO: proximal tubule-specific Foxo4-knockout; BUMPT cells: Boston University mouse kidney proximal tubular cells; NC: negative control; siRNA: small interfering RNA; Tcf12: Transcription factor 12; ChIP: chromatin immunoprecipitation; SMAD3: SMAD family member 3; P-SMAD3: phosphorylation -SMAD family member 3; TGF−β1: transforming growth factor beta 1; Igfbp3: Insulin-like growth factor-binding protein 3; Mmp13: matrix metalloproteinases 13; Ctgf: connective tissue growth factor; Pdgf: platelet-derived growth factor; SIS3: specific inhibitor of SMAD3.

Supplementary Material

Supplementary figures and tables.
https://www.ijbs.com/v23p0427s1.pdf

Acknowledgments

The work was supported by the National Natural Science Foundation of China (No. 82270734,82570820,82470730,82270733 and U25A2034). Zheng Dong was supported by the National Institutes of Health (5R01DK058831, 5R01DK087843, 1R01 DK129880, 1R01DK143226) and the Department of Veterans Affairs of USA (Senior Research Career Scientist award 1TK6BX005236, I01 BX000319).

Competing Interests

The authors have declared that no competing interest exists.

References

1. Pabla N, Dong Z. Cisplatin nephrotoxicity: mechanisms and renoprotective strategies. Kidney Int. 2008; 73: 994-1007.
2. Miller RP, Tadagavadi RK, Ramesh G, Reeves WB. Mechanisms of Cisplatin nephrotoxicity. Toxins (Basel). 2010; 2: 2490-518.
3. Holditch SJ, Brown CN, Lombardi AM, Nguyen KN, Edelstein CL. Recent Advances in Models, Mechanisms, Biomarkers, and Interventions in Cisplatin-Induced Acute Kidney Injury. Int J Mol Sci. 2019; 20.
4. Sears SM, Siskind LJ. Potential Therapeutic Targets for Cisplatin-Induced Kidney Injury: Lessons from Other Models of AKI and Fibrosis. J Am Soc Nephrol. 2021; 32: 1559-67.
5. Tang C, Livingston MJ, Safirstein R, Dong Z. Cisplatin nephrotoxicity: new insights and therapeutic implications. Nat Rev Nephrol. 2023; 19: 53-72.
6. Zhang X, Zhang Y, Liu Y. Fibroblast activation and heterogeneity in fibrotic disease. Nat Rev Nephrol. 2025; 21: 613-32.
7. Mylonas KJ, Ferenbach DA. Targeting Senescent Cells as Therapy for CKD. Kidney360. 2024; 5: 142-51.
8. Xu J, Zhou L, Liu Y. Cellular Senescence in Kidney Fibrosis: Pathologic Significance and Therapeutic Strategies. Front Pharmacol. 2020; 11: 601325.
9. Docherty MH, O'Sullivan ED, Bonventre JV, Ferenbach DA. Cellular Senescence in the Kidney. J Am Soc Nephrol. 2019; 30: 726-36.
10. Huang W, Hickson LJ, Eirin A, Kirkland JL, Lerman LO. Cellular senescence: the good, the bad and the unknown. Nat Rev Nephrol. 2022; 18: 611-27.
11. Chanvillard L, Mason T, Ferenbach DA. Understanding and targeting senescence in kidney disease. Clin Kidney J. 2025; 18: sfaf190.
12. Naved BA, Bonventre JV, Hubbell JA, Hukriede NA, Humphreys BD, Kesselman C, et al. Kidney repair and regeneration: perspectives of the NIDDK (Re)Building a Kidney consortium. Kidney Int. 2022; 101: 845-53.
13. Canaud G, Brooks CR, Kishi S, Taguchi K, Nishimura K, Magassa S, et al. Cyclin G1 and TASCC regulate kidney epithelial cell G(2)-M arrest and fibrotic maladaptive repair. Sci Transl Med. 2019; 11.
14. Ferenbach DA, Bonventre JV. Mechanisms of maladaptive repair after AKI leading to accelerated kidney ageing and CKD. Nat Rev Nephrol. 2015; 11: 264-76.
15. Li S, Livingston MJ, Ma Z, Hu X, Wen L, Ding HF, et al. Tubular cell senescence promotes maladaptive kidney repair and chronic kidney disease after cisplatin nephrotoxicity. JCI Insight. 2023; 8.
16. Liu W, Li Y, Luo B. Current perspective on the regulation of FOXO4 and its role in disease progression. Cell Mol Life Sci. 2020; 77: 651-63.
17. Fu Y, Xiang Y, Wei Q, Ilatovskaya D, Dong Z. Rodent models of AKI and AKI-CKD transition: an update in 2024. Am J Physiol Renal Physiol. 2024; 326: F563-F83.
18. Fu Y, Cai J, Li F, Liu Z, Shu S, Wang Y, et al. Chronic effects of repeated low-dose cisplatin treatment in mouse kidneys and renal tubular cells. Am J Physiol Renal Physiol. 2019; 317: F1582-F92.
19. Zheng H, Fang J, Lu W, Liu Y, Chen S, Huang G, et al. TCF12 regulates the TGF-beta/Smad2/3 signaling pathway to accelerate the progression of osteoarthritis by targeting CXCR4. J Orthop Translat. 2024; 44: 35-46.
20. Meng XM, Nikolic-Paterson DJ, Lan HY. TGF-beta: the master regulator of fibrosis. Nat Rev Nephrol. 2016; 12: 325-38.
21. Hong Q, Kim H, Cai GY, Chen XM, He JC, Lee K. Modulation of TGF-beta signaling new approaches toward kidney disease and fibrosis therapy. Int J Biol Sci. 2025; 21: 1649-65.
22. Abbad L, Esteve E, Chatziantoniou C. Advances and challenges in kidney fibrosis therapeutics. Nat Rev Nephrol. 2025; 21: 314-29.
23. Yang C, Chen XC, Li ZH, Wu HL, Jing KP, Huang XR, et al. SMAD3 promotes autophagy dysregulation by triggering lysosome depletion in tubular epithelial cells in diabetic nephropathy. Autophagy. 2021; 17: 2325-44.
24. Liu K, Yu M, He Y, Li Y, Huang XR, Li G, et al. Smad3 Mediates Renal Fibrosis via GPX4-Dependent Ferroptosis. Int J Biol Sci. 2025; 21: 5922-35.
25. He H, Wang H, Chen X, Zhong Y, Huang XR, Ma RC, et al. Treatment for type 2 diabetes and diabetic nephropathy by targeting Smad3 signaling. Int J Biol Sci. 2024; 20: 200-17.
26. Dan Hu Q, Wang HL, Liu J, He T, Tan RZ, Zhang Q, et al. Btg2 Promotes Focal Segmental Glomerulosclerosis via Smad3-Dependent Podocyte-Mesenchymal Transition. Adv Sci (Weinh). 2023; 10: e2304360.
27. de Keizer PL, Packer LM, Szypowska AA, Riedl-Polderman PE, van den Broek NJ, de Bruin A, et al. Activation of forkhead box O transcription factors by oncogenic BRAF promotes p21cip1-dependent senescence. Cancer Res. 2010; 70: 8526-36.
28. Baar MP, Brandt RMC, Putavet DA, Klein JDD, Derks KWJ, Bourgeois BRM, et al. Targeted Apoptosis of Senescent Cells Restores Tissue Homeostasis in Response to Chemotoxicity and Aging. Cell. 2017; 169: 132-47 e16.
29. Meng J, Li Y, Wan C, Sun Y, Dai X, Huang J, et al. Targeting senescence-like fibroblasts radiosensitizes non-small cell lung cancer and reduces radiation-induced pulmonary fibrosis. JCI Insight. 2021; 6.
30. Bourgeois B, Spreitzer E, Platero-Rochart D, Paar M, Zhou Q, Usluer S, et al. The disordered p53 transactivation domain is the target of FOXO4 and the senolytic compound FOXO4-DRI. Nat Commun. 2025; 16: 5672.
31. Chanda D, Otoupalova E, Smith SR, Volckaert T, De Langhe SP, Thannickal VJ. Developmental pathways in the pathogenesis of lung fibrosis. Mol Aspects Med. 2019; 65: 56-69.
32. Richeldi L, Collard HR, Jones MG. Idiopathic pulmonary fibrosis. Lancet. 2017; 389: 1941-52.
33. Bhardwaj S, Gautam RK, Kushwaha S. From senescence to scarring: Exploring TGF-beta signaling in cellular aging, fibrotic remodeling, and pulmonary fibrosis. Cytokine Growth Factor Rev. 2025; 86: 29-39.
34. Liu YH. Kidney Fibrosis: Fundamental Questions, Challenges, and Perspectives. INTEGRATIVE MEDICINE IN NEPHROLOGY AND ANDROLOGY. 2024; 11.
35. Ueda S, Tominaga T, Ochi A, Sakurai A, Nishimura K, Shibata E, et al. TGF-beta1 is involved in senescence-related pathways in glomerular endothelial cells via p16 translocation and p21 induction. Sci Rep. 2021; 11: 21643.
36. Rex N, Melk A, Schmitt R. Cellular senescence and kidney aging. Clin Sci (Lond). 2023; 137: 1805-21.
37. Li H, Fu P, Ma L. Therapeutic Application of Flavonoids in Kidney Disease and Senescence: Quercetin and Fisetin. INTEGRATIVE MEDICINE IN NEPHROLOGY AND ANDROLOGY. 2026; 13.
38. Cai J, Wei J, Zeng Y, Yi M, Zhou Y, Ai K, et al. UBC9-associated SUMOylation contributes to beta-catenin activation and kidney fibrosis. Kidney Int. 2025; 108: 642-57.
39. Cai J, Pan J, Zeng Y, Wei J, Yi M, Xiang Y, et al. SUMOylation protects against sepsis-associated acute kidney injury by stabilizing IkappaBalpha. Mol Ther. 2025.

40. Fu Y, Xiang Y, Wang Y, Liu Z, Yang D, Zha J, et al. The STAT1/HMGB1/NF-kappaB pathway in chronic inflammation and kidney injury after cisplatin exposure. Theranostics. 2023; 13: 2757-73.
41. Fu Y, Wang Y, Liu Y, Tang C, Cai J, Chen G, et al. p53/sirtuin 1/NF-kappaB Signaling Axis in Chronic Inflammation and Maladaptive Kidney Repair After Cisplatin Nephrotoxicity. Front Immunol. 2022; 13: 925738.
42. Emmons MF, Bennett RL, Riva A, Gupta K, Carvalho L, Zhang C, et al. HDAC8-mediated inhibition of EP300 drives a transcriptional state that increases melanoma brain metastasis. Nat Commun. 2023; 14: 7759.
43. Li L, Xiang T, Guo J, Guo F, Wu Y, Feng H, et al. Inhibition of ACSS2-mediated histone crotonylation alleviates kidney fibrosis via IL-1beta-dependent macrophage activation and tubular cell senescence. Nat Commun. 2024; 15: 3200.
44. Yin L, Deng Z, Liu J, Ye L, Huang J, Dai Y, et al. Keratin 20 Suppresses Exosomal Secretion of Peroxiredoxin 2 and Ferroptosis in Acute Kidney Injury. J Am Soc Nephrol. 2026; 37: 18-35.
45. Xu F, Jiang H, Li X, Pan J, Li H, Wang L, et al. Discovery of PRDM16-Mediated TRPA1 Induction as the Mechanism for Low Tubulo-Interstitial Fibrosis in Diabetic Kidney Disease. Adv Sci (Weinh). 2024; 11: e2306704.